Unified treatment of scattering and cluster structure in α+closed shell nuclei: ^{20}Ne and ^{44}Ti

B. Buck and J. C. Johnston
Department of Physics, University of Oxford, Theoretical Physics, 1 Keble Road, Oxford OX1 3NP, United Kingdom

A. C. Merchant and S. M. Perez*
Department of Physics, University of Oxford, Nuclear Physics Laboratory, Keble Road, Oxford OX1 3RH, United Kingdom
(Received 20 March 1995)

The model of an α cluster orbiting a closed shell core provides a highly successful description of low lying bound and resonant states of ^{20}Ne and has been successfully extended to ^{44}Ti by various authors. This description is closely related to α scattering from the relevant closed shell core, and although the scattering has previously been reasonably well reproduced with a local optical model potential, few attempts have been made to link the two phenomena. In this paper, a universal α-core interaction is given which describes the spectra, $B(E2\downarrow)$ transition strengths, α-decay widths, and differential elastic scattering cross sections for the systems corresponding to ^{20}Ne=^{16}O+α and ^{44}Ti=^{40}Ca+α. This potential has only a single free parameter, the radius, whose value is kept fixed for each nucleus.

PACS number(s): 21.60.Gx, 23.20.Lv, 23.60.+e, 25.55.Ci

I. INTRODUCTION

The simplest possible binary cluster model has been shown to account well for many of the observed features of various light nuclei. The basic assumption of this model is that such nuclei can be described accurately in terms of a system of two component nuclei, each with its free state characteristics, interacting through a deep local potential. Here we shall discuss in detail the description of ^{20}Ne and ^{44}Ti, treated as ^{16}O+α and ^{40}Ca+α, respectively. A reasonable approximation to the local potential is obtained from the double folding model [1,2]. The cluster state energies and wave functions are then obtained by solution of the Schrödinger equation. The Pauli exclusion principle is taken into account by placing restrictions on the values of the radial and angular momentum quantum numbers N and L. An adequate treatment is found by using the oscillator shell model. The number of excitation quanta in the orbital motion is given by $G=2N+L$. To include antisymmetry effects G must be restricted to values greater than $\Sigma_c(2n_c+l_c)$, where n_c and l_c are the single particle quantum numbers of the cluster nucleons, which are excluded from levels below the Fermi energy of the core.

The deep local potential can also be identified with the real part of the optical potential which describes the elastic scattering of the cluster and the core; hence the binary cluster model should be consistent with the elastic scattering reactions ^{16}O(α,α)^{16}O [3] and ^{40}Ca(α,α)^{40}Ca [4]. Previous attempts to unify bound state and scattering descriptions have restricted attention to a single nucleus [2,3], and although a fixed potential geometry was employed, it was found necessary to have somewhat different depths for the associated potentials when dealing with the two phenomena.

Our consistent view is made possible by a new potential parametrization, in which the deep local potential is independent of energy and angular momentum and, except for the radius, employs the same parameter values for both ^{20}Ne and ^{44}Ti. The present work goes beyond our previous studies of α+double closed shell core nuclei [5] by calculating the low energy elastic scattering in detail, rather than simply comparing our proposed real potentials with previously fitted optical potentials.

II. EXPERIMENTAL DATA

In ^{20}Ne and ^{44}Ti the energies of all members of the ground state $K^\pi=0^+$ bands are known up to their terminations at $L=G$ (with $G=8$ and 12, respectively). The energies of the lower states of the $K^\pi=0^-$ bands (with $G=9$ and 13, respectively) and are also known with confidence. In ^{20}Ne there is some ambiguity over which of the observed 7^- and 9^- states are the uppermost members of the $K^\pi=0^-$ band. Our model does not make a clear prediction for the correct members and it is believed that there may be significant mixing with neighboring 7^- and 9^- levels of different structure. Furthermore, in ^{44}Ti the 7^-, 9^-, 11^-, and 13^- members of the $G=13$, $K^\pi=0^-$ band, which are predicted by the cluster model, have not yet been observed. Here we estimate the positions and widths of these levels and expect that their eventual observation will provide further evidence for the cluster model.

The α decay widths for the cluster states which lie above threshold in ^{20}Ne have been measured, but unfortunately none is available in ^{44}Ti. A complete set of values for this nucleus would be of great assistance, especially in the identification of the 12^+ member of the $K^\pi=0^+$ band. The elastic scattering of both ^{16}O(α,α)^{16}O [3] and ^{40}Ca(α,α)^{40}Ca [4] has been well investigated over a large range of angles and energies, with the bulk of the data for the α+^{16}O system taken below 30 MeV incident energy. This is because the main motivation for exploring that system was to investigate the low lying resonances.

*Permanent address: Department of Physics, University of Cape Town, Private Bag, Rondebosch 7700, South Africa.

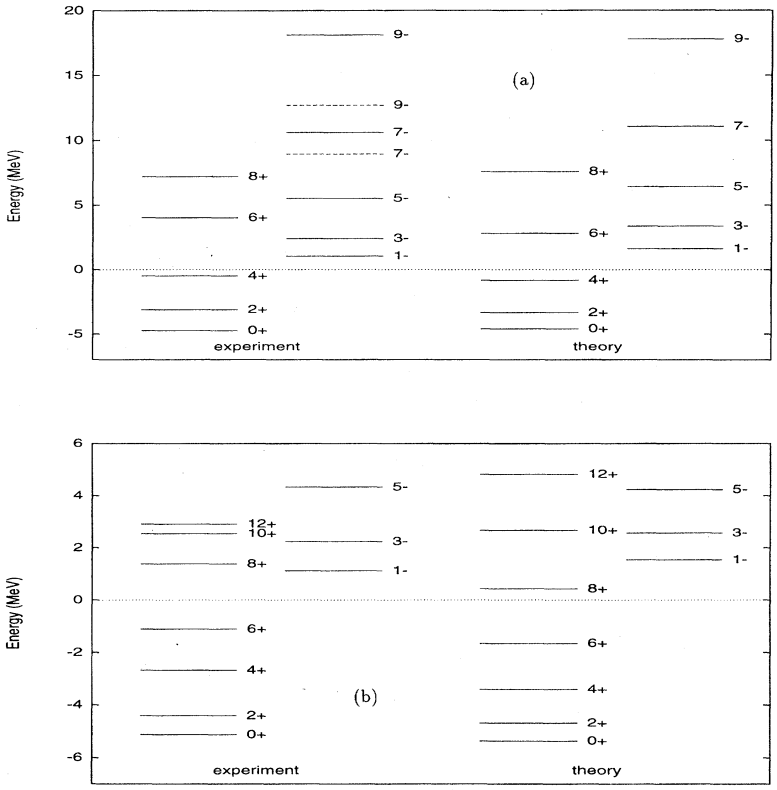

FIG. 1. Experimental energy scheme for the $K^{\pi}=0^{+}$ and $K^{\pi}=0^{-}$ bands, together with the results of our model calculation for ^{20}Ne [upper frame (a)] and for ^{44}Ti [lower frame (b)].

III. α-CORE POTENTIAL

The new shape that we propose [5] has the form:

$$V(r)=-V_0\left[\frac{\alpha}{1+\exp[(r-R_v)/a_v]}+\frac{1-\alpha}{(1+\exp[(r-R_v)/3a_v])^3}\right]. \quad (1)$$

This form has evolved through trial and error, and is the best that has been tried so far. We do not claim that it is optimal, but we believe that it reproduces all the available data well enough to represent a significant improvement on previous parametrizations and to suggest that there does indeed exist a universal energy-independent potential shape. A further project using Bayesian inversion techniques is in progress to find this shape more exactly. The parameters are fixed to the following values:

$$V_0=250 \text{ MeV}, \quad a_v=0.73 \text{ fm}, \quad \alpha=0.3. \quad (2)$$

TABLE I. α-emission widths in ^{20}Ne.

J^{π}	E^* (MeV)	R_v (fm)	$\Gamma_{\alpha}^{\text{calc}}$ (keV)	$\Gamma_{\alpha}^{\text{expt}}$ (keV)
6^+	8.776	3.015	0.081	0.11 ± 0.02
8^+	11.951	3.072	0.055	0.035 ± 0.010
1^-	5.788	3.093	0.049	0.028 ± 0.003
3^-	7.156	3.117	15.7	8.2 ± 0.3
5^-	10.262	3.111	255	145 ± 40
7^-	13.692	3.165	218	158 ± 15
9^-	17.430	3.234	38	53 ± 6
7^-	15.336	3.087	764	78 ± 7
9^-	22.87	3.053	892	$\leqslant 225\pm40$
0^+	7.85 [a]	3.060	1770	>800
2^+	8.71 [a]	3.060	2620	>800

[a]Predicted energies.

TABLE II. Estimated α-emission widths in ^{44}Ti.

J^{π}	E^* (MeV)	R_v (fm)	$\Gamma_{\alpha}^{\text{calc}}$ (keV)
8^+	6.51	4.301	$\ll 0.001$
10^+	7.67	4.334	$\ll 0.001$
12^+	8.04	4.378	$\ll 0.001$
1^-	6.25	4.348	$\ll 0.001$
3^-	7.37	4.344	$\ll 0.001$
5^-	9.46	4.326	0.039
7^-	11.61 [a]	4.330	0.454
9^-	14.31 [a]	4.330	0.995
11^-	17.28 [a]	4.330	0.446
13^-	20.21 [a]	4.330	0.037
0^+	11.05 [a]	4.330	233
2^+	11.66 [a]	4.330	332

[a]Predicted energies.

TABLE III. $B(E2\downarrow)$ values. Calculated and measured $B(E2\downarrow)$ values (in e^2 fm^4) for ^{20}Ne and ^{44}Ti.

Nucleus	Transition	$B(E2\downarrow)_{\text{calc}}$	$B(E2\downarrow)_{\text{expt}}$
^{20}Ne	$2^+(1.63\text{ MeV}) \rightarrow 0^+(0.00\text{ MeV})$	48	68 ± 4
	$4^+(4.25\text{ MeV}) \rightarrow 2^+(1.63\text{ MeV})$	62	71 ± 7
	$6^+(8.78\text{ MeV}) \rightarrow 4^+(4.25\text{ MeV})$	53	65 ± 10
	$8^+(11.95\text{ MeV}) \rightarrow 6^+(8.78\text{ MeV})$	29	30 ± 4
	$3^-(7.16\text{ MeV}) \rightarrow 1^-(5.79\text{ MeV})$	174	164 ± 26
^{44}Ti	$2^+(1.08\text{ MeV}) \rightarrow 0^+(0.00\text{ MeV})$	103	120 ± 37
	$4^+(2.45\text{ MeV}) \rightarrow 2^+(1.08\text{ MeV})$	140	277 ± 55
	$6^+(4.02\text{ MeV}) \rightarrow 4^+(2.45\text{ MeV})$	135	157 ± 28
	$8^+(6.51\text{ MeV}) \rightarrow 6^+(4.02\text{ MeV})$	111	>14
	$10^+(7.67\text{ MeV}) \rightarrow 8^+(6.51\text{ MeV})$	76	138 ± 28
	$12^+(8.04\text{ MeV}) \rightarrow 10^+(7.67\text{ MeV})$	37	<60

The only parameter that was varied between the two nuclei was the radius R_v and the values used are 3.06 fm for $\alpha+^{16}$O and 4.33 fm for $\alpha+^{40}$Ca.

A. Cluster state spectra

The energies and wave functions of the bound states were found by solving the Schrödinger equation, subject to the Pauli restrictions mentioned above, and those of the resonant states were calculated in similar fashion by rounding off the potential at its maximum so as to render them effectively bound also. The fitting to the observed spectra was then done using a least squares procedure.

In ^{20}Ne there are two possible sets of values for the energies of the 7^- and 9^- members of the $K^\pi=0^-$ band. When the excitation energies were taken to be $E(7^-)=15.34$ MeV and $E(9^-)=22.87$ MeV [6], rather than $E(7^-)=13.69$ MeV and $E(9^-)=17.43$ MeV [7], the spectrum fit was found to be significantly better. With this choice the model reproduces the main features of both the positive and negative parity bands using the single potential defined above, with $R_v=3.06$ fm [see Fig. 1(a)]. This potential also results in a higher nodal band, with $G=2N+L=10$, whose lowest members are in good agreement (see Table I) with the positions and widths of the corresponding members of the $K^\pi=0_4^+$ band in ^{20}Ne. The latter, with $E(0^+)\sim8.7$ MeV and $E(2^+)\sim8.8$ MeV, and widths >800 keV in each case, are believed to have a strong α-cluster character [3].

The known states of ^{44}Ti were fitted well with $R_v=4.33$ fm, apart from the 12^+ state [see Fig. 1(b)]. However, there may be an additional 12^+ state [8] close to the predicted energy. This could be the true member of the $K^\pi=0^+$ band, but even if the terminating band member has already been identified correctly, it seems reasonable that the proximity of two (or more) such states would produce mixing and so lead to the observed discrepancy in position. Once the bandhead has been correctly positioned, the compression of the band, when compared with a purely rotational structure, is well reproduced. The correct positioning of both the positive and negative parity bands with a parity independent potential is also an improvement on most earlier works [2,9,10]. Furthermore, likely candidates for the lowest members of the $G=2N+L=14$ higher nodal band are resonances found at $E(0^+)\sim11.1$ MeV and $E(2^+)\sim12.1$ MeV, with widths of 550 keV and 300 keV, respectively [2,11]. These are reasonably reproduced here (see Table II).

B. α-decay widths

The α-decay widths of the cluster states in ^{20}Ne were evaluated by calculating phase shifts as a function of energy using a standard optical model code, and checked by a complex eigenvalue method [12] and by a semiclassical calculation. In order to do this accurately the predicted and observed energy levels must be at the same energy. This requires minor tuning of the potential by slightly altering R_v for each level, all the other parameters being fixed by Eq. (2). The results shown in Table I agree quite well with experiment but, in contradiction with the results of the energy fitting above, show a clear preference for an assignment of $J^\pi=7^-$ and 9^- members of the $K^\pi=0^-$ band to the experimental states at 13.69 and 17.43 MeV excitation energies, respectively. The latter are now accepted [7] as the correct members of the $K^\pi=0^-$ band, and the present results indicate significant mixing between the pairs of 7^- and 9^- states.

Similar calculations for the states in ^{44}Ti above the ^{40}Ca-α threshold indicate that the 8^+, 10^+, 12^+, 1^-, and 3^- are all very narrow ($\Gamma_\alpha\ll1$ eV). The widths for the remaining negative parity states, most of which have not yet been detected, are listed in Table II. So far, no experimental partial α widths are available for any of the proposed α-cluster states in ^{44}Ti.

C. $B(E2\downarrow)$ transition strengths

Table III compares our calculated $B(E2\downarrow)$ reduced transition strengths with measured values for ^{20}Ne and ^{44}Ti. We calculate these strengths with wave functions obtained from our previous solutions of the Schrödinger equation, without introducing any effective charges. We have [5]

$$B(E2;\ G,L\rightarrow L-2)=\frac{15}{8\pi}\beta_2^2\frac{L(L-1)}{(2L+1)(2L-1)}\langle r_{L,L-2}^2\rangle^2 \tag{3}$$

for a transition from L to $L-2$ involving spinless clusters and cores where

$$\beta_2=\frac{Z_1A_2^2+Z_2A_1^2}{(A_1+A_2)^2}, \tag{4}$$

with (Z_1,A_1) and (Z_2,A_2) the (charge, mass) numbers of the cluster and core. The agreement between the theoretical calculations and the experimental data is generally very good.

We also calculate ground state charge radii for ^{20}Ne and ^{44}Ti from our cluster model by evaluating

$$\langle R_{\rm ch}^2\rangle = \frac{Z_1}{Z_1+Z_2}\langle R_1^2\rangle + \frac{Z_2}{Z_1+Z_2}\langle R_2^2\rangle + \frac{\beta_2}{Z_1+Z_2}\langle r_{00}^2\rangle, \quad (5)$$

where $\langle R_1^2\rangle$ and $\langle R_2^2\rangle$ are the mean square charge radii of the cluster and core, and $\langle r_{00}^2\rangle$ is the expectation value of the squared cluster-core separation distance taken between ground state relative motion wave functions. Using values for cluster and core charge radii from the tabulation of De Vries *et al.* [13] we obtain a root mean square charge radius for ^{20}Ne of 3.002 fm (cf. measured values between 2.992 and 3.040 fm [13]) and for ^{44}Ti of 3.593 fm (cf. measured values for ^{48}Ti and ^{50}Ti between 3.573 and 3.713 fm [13]).

D. Elastic α scattering

The elastic scattering differential cross sections were calculated using a standard optical model code. In general, some care should be taken when choosing how best to fit the parameters of the optical potential. Standard χ^2 fits based on experimental errors alone are to some extent flawed, because they do not take into account the accuracy to which a potential model description may reasonably be expected to fit elastic scattering data. As a parallel, in fitting energy levels in a potential model, it is clearly inappropriate to base the fit on the (tiny) experimental errors associated with the levels. Thus the concept of theoretical error must be introduced, and its form decided on.

TABLE IV. Imaginary potential depths W_0 [see Eqs. (7) and (8)].

$\alpha+^{16}$O		$\alpha+^{40}$Ca	
E (MeV)	W_0 (MeV)	E (MeV)	W_0 (MeV)
22.0	2.2	24.1	22.1
25.4	3.9	29.0	24.8
26.6	5.7	39.6	31.8
30.0	5.0	49.5	38.7
39.3	7.1		
49.5	9.9		

The most probable distribution for any variable of finite variance, with no other constraints, is a Gaussian [14]. The variance itself is not determined by these considerations. The only guide to the form of the variance is the acceptability of the fits that we obtain.

The data come in two forms: absolute values of the differential cross sections (in mb/sr) and as the ratio of the differential cross section to the Rutherford value. In the case of the ratio to Rutherford values it was adequate to assign a constant variance to each data point at a given energy. This leads to the familiar least squares fitting. However, this procedure does not give sensible results for the case of absolute values of the differential cross section because of the large range of values this takes on. In this case it was found nec-

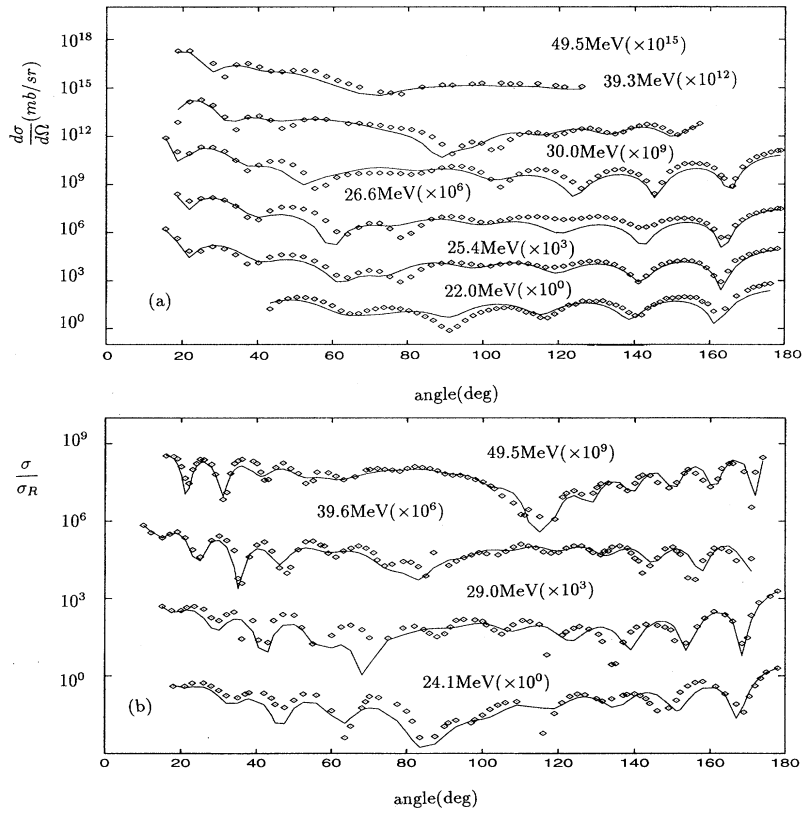

FIG. 2. Fits to the elastic α-scattering differential cross sections at various energies for ^{16}O (α,α) ^{16}O [upper frame (a)] and ^{40}Ca(α,α) ^{40}Ca [lower frame (b)].

essary to take the standard deviations of the data points to be proportional to the value of the cross section (i.e., to have a fixed percentage error assigned to each data point). The quantity that must now be minimized is

$$L=\sum_i \left[\frac{\left(\frac{d\sigma}{d\Omega}\right)_i^{\text{expt}} - \left(\frac{d\sigma}{d\Omega}\right)_i^{\text{theor}}}{\left(\frac{d\sigma}{d\Omega}\right)_i^{\text{expt}}} \right]^2 \quad (6)$$

where $(d\sigma/d\Omega)_i^{\text{expt}}$ is the observed value at the ith angle and $(d\sigma/d\Omega)_i^{\text{theor}}$ is the predicted value at the ith angle.

The real part of the optical model potential was taken to be that of Eq. (1), and the imaginary part was taken to have a surface peaked Woods-Saxon derivative form

$$W(r)=\frac{-4W_0\exp[(r-R_w)/a_w]}{\{1+\exp[(r-R_w)/a_w]\}^2} \quad (7)$$

for the $\alpha+{}^{16}$O system, and a squared Woods-Saxon form

$$W(r)=\frac{-W_0}{\{1+\exp[(r-R_w)/2a_w]\}^2} \quad (8)$$

for the $\alpha+{}^{40}$Ca system. It is well known that the fit is insensitive to the precise form of the imaginary part of the potential. The choice of these forms was therefore somewhat arbitrary. However, with these choices we have been able to confine the energy dependence of $W(r)$ to the depth parameter W_0 (see Table IV for the fitted values). The other two parameters R_w and a_w were kept fixed. In fact, R_w was constrained to be equal to the radius parameter of the real potential R_v and a_w was held constant at 1.0 fm.

First, the fitting was done using $\alpha=0.3$ in Eq. (1) and varying the parameters V_0, a_v, R_v, W_0, for the $\alpha+{}^{40}$Ca system for each observed energy over a large range. There was a significant discrete ambiguity in the values of the parameters, but there was only one choice for which V_0, a_v, and R_v were approximately energy independent, with average values consistent with the values deduced from the energy level analysis of ^{44}Ti. With real well parameters thus fixed at $V_0=250$ MeV, $a_v=0.73$ fm, and $R_v=4.33$ fm, and imaginary well parameters fixed at $R_w=R_v$ and $a_w=1.00$ fm, the fits were repeated with the imaginary well depth as the only free parameter, with the results shown in Table IV and Fig. 2. Fitting of the $\alpha+{}^{16}$O data was now straightforward. All parameters except $R_v=R_w=3.06$ fm and W_0 were fixed at the values found for the $\alpha+{}^{40}$Ca system. With the potential thus restricted both the energy levels of ^{20}Ne and the $\alpha+{}^{16}$O scattering were accurately reproduced up to 30 MeV. Moreover, the general features of the scattering were reproduced up to a value of about 50 MeV, as can be seen from our final results displayed in Fig. 2.

IV. CONCLUSION

The differential cross sections of the scattering of α particles on ^{16}O and ^{40}Ca have been analyzed in the framework of the optical model, and the spectra, $B(E2\downarrow)$ transition strengths, and α-decay widths of the cluster states in ^{20}Ne and ^{44}Ti nuclei have been modeled in terms of an α particle + closed shell core. The analysis of all these phenomena was performed consistently, using a single real potential shape with energy and angular momentum independent parameters, with only the radius changing from one nucleus to the other. The success of this potential shape, in both nuclei, strongly suggests the existence of a universal potential.

ACKNOWLEDGMENTS

J.C.J. and A.C.M. would like to thank the U.K. Engineering and Physical Sciences Research Council (EPSRC) for financial support. We also thank Dr. F. Michel for sending us his $\alpha+{}^{16}$O and $\alpha+{}^{40}$Ca elastic scattering data.

[1] B. Buck, C. B. Dover, and J. P. Vary, Phys. Rev. C **11**, 1803 (1975).
[2] F. Michel, G. Reidemeister, and S. Ohkubo, Phys. Rev. Lett. **57**, 1215 (1986); Phys. Rev. C **37**, 292 (1988).
[3] F. Michel, J. Albinski, P. Belery, Th. Delbar, C. Grégoire, B. Tasiaux, and G. Reidemeister, Phys. Rev. C **28**, 1904 (1983).
[4] Th. Delbar, C. Grégoire, G. Paic, R. Ceulneer, F. Michel, R. Vanderpoorten, A. Budzanowski, H. Dabrowski, L. Freindl, K. Grotowski, S. Micek, R. Planeta, A. Strzalkowski, and K. Eberhard, Phys. Rev. C **18**, 1237 (1978).
[5] B. Buck, A. C. Merchant, and S. M. Perez, Phys. Rev. C **51**, 559 (1995).
[6] F. Ajzenberg-Selove, Nucl. Phys. **A392**, 1 (1983).
[7] F. Ajzenberg-Selove, Nucl. Phys. **A475**, 1 (1987).
[8] F. Haas (private communication).
[9] T. Wada and H. Horiuchi, Phys. Rev. Lett. **58**, 2190 (1987); Phys. Rev. C **38**, 2063 (1988).
[10] A. C. Merchant, K. F. Pal, and P. E. Hodgson, J. Phys. G **15**, 601 (1989).
[11] D. Frekers, R. Santo, and K. Langanke, Nucl. Phys. **A394**, 189 (1983).
[12] T. Vertse, K. F. Pal, and Z. Balogh, Comput. Phys. Commun. **27**, 309 (1982).
[13] H. De Vries, C. W. De Jaeger, and C. De Vries, At. Data Nucl. Data Tables **36**, 495 (1987).
[14] B. Buck, in *Maximum Entropy in Action*, edited by B. Buck and V. A. Macaulay (Clarendon Press, Oxford, 1991).